Journal of Magnetic Resonance **147,** 43–58 (2000)
doi:10.1006/jmre.2000.2160, available online at http://www.idealibrary.com on IDEAL®

Effects of Various Types of Molecular Dynamics on 1D and 2D ^{2}H NMR Studied by Random Walk Simulations

M. Vogel and E. Rössler

Physikalisches Institut, Univerversität Bayreuth, D-95440 Bayreuth, Germany

Received November 1, 1999; revised July 21, 2000

By carrying out random walk simulations we systematically study the effects of various types of complex molecular dynamics on ^{2}H NMR experiments in solids. More precisely, we calculate one-dimensional (1D) ^{2}H NMR spectra and the results of two dimensional (2D) ^{2}H NMR experiments in time domain, taking into account isotropic as well as highly restricted motions which involve rotational jumps about different finite angles. Although the dynamical models are chosen to mimic the primary and secondary relaxation in supercooled liquids and glasses, we do not intend to describe experimental results quantitatively but rather to show general effects appearing for complex reorientations. We carefully investigate whether 2D ^{2}H NMR in time domain, which was originally designed to measure correlation times of ultraslow motions ($\tau \geq 1$ ms), can be used to obtain shorter τ, too. It is demonstrated that an extension of the time window to $\tau \geq 10$ μs is possible when dealing with exponential relaxation, but that it will fail if there is a distribution of correlation times $G(\lg\tau)$. Vice versa, we show that 1D ^{2}H NMR spectra, usually recorded to look at dynamics with τ in the microsecond regime, are also applicable for studying ultraslow motions provided that the loss of correlation is achieved step by step. Therefore, it is useful to carry out 1D and 2D NMR experiments simultaneously in order to reveal the mechanism of complex molecular motions. In addition, we demonstrate that highly restricted dynamics can be clearly observed in 1D spectra and in 2D NMR in time domain if long solid-echo delays and large evolution times are applied, respectively. Finally, unexpected observations are described which appear in the latter experiment when considering very broad distributions $G(\lg\tau)$. Because of these effects, time scale and geometry of a considered motion cannot be extracted from a straightforward analysis of experimental results.

Key Words: **1D ^{2}H NMR; 2D ^{2}H NMR; random walk simulations; molecular dynamics; disordered systems.**

1. INTRODUCTION

NMR is well suited to study slow molecular dynamics in solids. In particular, various ^{2}H NMR techniques have proved valuable tools for such investigations (*1*). One-dimensional (1D) ^{2}H NMR spectra are usually recorded to analyze molecular reorientations with correlation times on the order of the inverse quadrupolar coupling constant, i.e., in the microsecond regime. On the other hand, applying two-dimensional (2D) ^{2}H NMR, it is possible to look at ultraslow motions which are typically characterized by time constants in the range from about a few milliseconds to some seconds. For example, using 2D ^{2}H NMR in time domain allows one to measure the correlation function f_2 of the second Legendre polynomial, where the latter describes the molecular orientation (*2*). Thus, the corresponding correlation time τ of ultraslow reorientations is directly accessible.

In the first applications of 1D and 2D ^{2}H NMR, comparatively simple types of molecular dynamics were studied or, at least, simple dynamical models were used in an analysis of the results. Concerning 1D spectra, rotational jumps occurring about a single axis and among a small number of sites were mainly under investigation, e.g., π flips (*3, 4*) or $2\pi/3$ (*5*) and $2\pi/5$ jumps (*6*). Sometimes, small angle fluctuations about the jump axis (*7–9*) or a wobbling of the axis itself (*10*) were additionally taken into account. In the early days of 2D ^{2}H NMR, similar kinds of motion were considered (*11–15*). When looking at isotropic dynamics, the model of isotropic rotational diffusion was applied to simulate measured 1D and 2D spectra, respectively (*1, 16*). Only recently, 2D NMR in time domain was also used to reveal the mechanism of more complex molecular dynamics, i.e., rotational jumps taking place about various axes and involving different finite jump angles (*17–20*).

In a forthcoming publication, we will study complex molecular dynamics connected with the primary and secondary relaxation in supercooled liquids and glasses by applying 1D and 2D ^{2}H NMR experiments (*21*). However, due to the complicated properties of these motions and the structure of the involved pulse sequences, unexpected findings appear in this inquiry which make a straightforward analysis of the results impossible. For a better understanding of these experimental observations, we will here systematically investigate the effects of various types of complex molecular dynamics on ^{2}H NMR measurements by carrying out simulations. More precisely, we calculate the results of 1D ^{2}H NMR spectra and of 2D ^{2}H NMR experiments in time domain. Such a systematic investigation is, to our knowledge, still missing for complex molecular dynamics although such motions exist in a lot of fields, for example, as aforementioned, at the liquid to glass

1090-7807/00 $35.00

transition. In order to calculate the relevant NMR observables in our study we carry out random walk (RW) simulations, since this technique has recently proved well suited to describe complicated motions (*18–20, 22*). We use dynamical models reflecting the actual molecular dynamics in supercooled liquids and glasses to some extent. This choice is intended to allow an easy comparison of the results obtained in the RW simulations and in our ^{2}H NMR experiments (*21*), respectively. However, we do not plan to describe the experimental findings quantitatively, but rather we will try to keep the models as simple as possible in order to stress the general aspects. Another goal of this publication is to study the limits of the time windows of ^{2}H NMR measurements. Such an analysis is not only of methodical interest but also of practical importance when considering supercooled liquids, as will be demonstrated. We note that, although we solely deal with ^{2}H NMR, the results of our investigation are not limited to deuterons but can be transferred to other nuclei with a dominating single particle interaction as well.

According to our goal, we want to simulate molecular motions typical of reorientations in supercooled liquids and glasses. Therefore, we have to summarize the main features of molecular dynamics in such samples at this point. It is well known that the isotropic main relaxation in supercooled liquids (α process) is strongly temperature dependent (*23*) and characterized by a distribution of correlation times $G(\lg\tau)$ (*24*). Moreover, 2D ^{2}H NMR experiments in time domain (*17–20*) and other multidimensional NMR studies (*25*) have yielded valuable information about the mechanism of molecular reorientations involved in the α process. It has turned out that there is a gradual loss of correlation which is achieved by many elementary rotational jumps about various finite jump angles taking place one after another. This means that the elementary reorientations are characterized by a jump correlation time τ_j which is much shorter than the correlation time τ. Often, there is a secondary relaxation called Johari-Goldstein-β process in supercooled liquids and glasses, too (*26*). This secondary relaxation survives even below the liquid to glass transition, i.e., at temperatures where the α process is already frozen in. The β process is mostly regarded as a highly restricted motion and described by a very broad distribution of correlation times (*26, 27*).

Having in mind these observations in supercooled liquids and glasses, the problems to be tackled become obvious. First, whether the time windows of 2D ^{2}H NMR experiments can be enlarged should be studied. Besides the methodical importance, such an extension seems to be particularly useful for supercooled liquids due to the broad distributions $G(\lg\tau)$ and the strong temperature dependence of molecular dynamics in these substances. Whereas the upper limit of the time window is determined by the spin–lattice relaxation and, thus, depending on sample and temperature fixed on the order of hundreds of milliseconds or some seconds, the lower boundary can in principle be shifted by almost 3 decades from roughly 1 ms to a few microseconds when applying a recently developed additional phase cycle (*28*). However, when studying dynamics on the microsecond time scale by 2D NMR one has to keep in mind that molecular reorientations occur during the frequency detection. As has been shown, this fact complicates the analysis of 2D ^{2}H NMR spectra (*29, 30*). On the other hand, the information content of 2D NMR experiments in time domain under these circumstances has not yet been investigated in a systematic manner. Therefore, we will here follow the question of whether the correlation function f_2 can be measured even for τ on the order of microseconds using 2D ^{2}H NMR in time domain. As will become obvious, the results of this study are strongly influenced by the fact that, for experimental reasons, a four-pulse instead of the usual three-pulse sequence must be applied in ^{2}H NMR (*1*).

As aforementioned, another intention of the present paper is to study the effects of complex molecular reorientations on the lineshape of 1D ^{2}H NMR spectra. In particular, dynamical models typical of the relaxations in supercooled liquids and glasses shall be considered. Consequently, when looking at the α process, 1D NMR spectra for isotropic rotational jumps about various finite angles have to be calculated. However, such simulations go beyond the above-mentioned prior efforts. Therefore, we will here demonstrate that 1D spectra in the presence of complex molecular dynamics can easily be calculated by carrying out RW simulations. These RW simulations have been used in NMR so far only when evaluating results of 2D experiments in time domain (*18–20*).

Having tackled these more general tasks concerning 1D and 2D ^{2}H NMR experiments, one can investigate in detail how these measurements are affected by various dynamical models. Above all, it is interesting to look at the meaning of the jump correlation time τ_j in the case of motions like the α process where the time scales of τ and τ_j are different. For the present investigation, it is useful to distinguish three cases:

- case 1: $\tau, \tau_j > T_2^*$;
- case 2: $\tau > T_2^* > \tau_j$;
- case 3: $T_2^* > \tau, \tau_j \geq 1/\delta$.

Here, δ represents the anisotropy parameter of the quadrupolar interaction for deuterons, cf. Eq. [1], and T_2^* the time constant of the spin–spin relaxation in the absence of motion, i.e., considering ^{2}H NMR the time constant of the decay caused by the static dipole–dipole interaction. In supercooled liquids and glasses, T_2^* is typically on the order of several hundreds of microseconds. The first case, $\tau, \tau_j > T_2^*$, corresponds to the dynamical range for which usually the terms "ultraslow motion" or "slow motion limit" are applied. Such motions can easily be studied by 2D NMR (*1*). Case 3 is often called "intermediate motional regime." This interval agrees with the time window of 1D NMR (*3*). Here, we will mainly deal with cases 2 and 3 because of their importance for supercooled liquids and glasses. In case 2, the correlation time τ lies right in the time window of 2D ^{2}H NMR, whereas the jump corre-

lation time is found in the one of 1D ^{2}H NMR. Therefore, it is interesting to study whether motions where the time scales of τ and τ_j are separated can simultaneously be observed in 1D and 2D NMR. We mention that such a scenario is reported for the limit of isotropic rotational diffusion where the difference of both time scales tends to infinity (*16*).

Finally, since the β process in glasses is believed to be a highly restricted motion, it is necessary to investigate the influence of such dynamics on ^{2}H NMR measurements, too. It is known that small angle fluctuations do not strongly affect 1D (*9*) and 2D (*1*) ^{2}H NMR spectra recorded in the usual way using short echo delays. Here we show that, nevertheless, they can be observed both in the 1D spectral lineshape and in 2D ^{2}H NMR in time domain under certain circumstances. Moreover, we extensively discuss unexpected effects appearing in the latter experiment if there is a very broad distribution of correlation times for a highly restricted motion, as is typical of the β process.

2. THEORY

Applying solid-state ^{2}H NMR the NMR frequency in the rotating frame ω_Q depends on the orientation of the quadrupolar coupling tensor with respect to the external static magnetic field $\mathbf{B}_0$. Considering covalent C–D bonds, e.g., in deuterated organic compounds, the quadrupolar coupling tensor is symmetric and its principal z-axis points along the direction of the bond. In this case, the NMR frequency is given by

$$\omega_Q(\theta(t)) = \pm\frac{\delta}{2}(3\cos^2\theta(t) - 1) \quad \eta = 0, \qquad [1]$$

where the anisotropy parameter δ is typically $2\pi \times 125$ kHz and θ represents the angle between $\mathbf{B}_0$ and the C–D bond. Thus, ω_Q and the orientation of the bond axis are connected via the second Legendre polynomial $P_2(\cos\theta)$ and molecular reorientations cause a variation of the NMR frequency.

1D ^{2}H NMR spectra can be recorded by applying the solid-echo pulse sequence. It consists of two $\pi/2$ pulses which are separated by an echo delay t_p and shifted in phase by $\pi/2$. Assuming perfect RF pulses and neglecting spin–spin relaxation, the signal S measured at a time $t \geq 2t_p$ in the solid-echo sequence is proportional to (*3*)

$$S_{t_p}(t) \propto \langle\cos\{\phi(0, t_p) - [\phi(t_p, 2t_p) + \phi(2t_p, t)]\}\rangle, \qquad [2]$$

where the phases ϕ are calculated according to

$$\phi(t_1, t_2) = \int_{t_1}^{t_2} \omega_Q(t')dt' \qquad [3]$$

and the brackets $\langle\ldots\rangle$ denote the ensemble average. If molecular dynamics during the pulse sequence can be neglected, ω_Q will be constant and we can rewrite Eq. [2] as $S_{t_p}(t) \propto \langle\cos\{\omega_Q(t - 2t_p)\}\rangle$. Obviously, an echo appears at $t = 2t_p$ and the lineshape of the 1D spectrum, obtained by a Fourier transformation starting at the echo maximum, is independent of the applied echo delay t_p. In contrast, if molecular reorientations take place during the pulse sequence a time-dependent $\omega_Q(t)$ results. Under these circumstances, a reduced amplitude of the echo and changes in the lineshape of the 1D spectra are observed which depend both on the kind of motion and on the echo delay t_p (*3–10*).

2D ^{2}H NMR experiments in time domain can in principle be carried out by applying a three-pulse sequence with proper experimental parameters. For example, using the Jeener–Broekaert sequence, $(\pi/2)_y$–t_p–$(\pi/4)_x$–t–$(\pi/4)_x$–t_2, it is possible to create a stimulated echo at a time $t_2 = t_p$ (*31*). Evaluating the amplitude of the stimulated echo for various mixing times $t \gg t_p$ and considering ultraslow motions (case 1), a two-time correlation function

$$F^{\sin}_{t_p}(t) \propto \langle\sin[\omega_Q(0)t_p]\sin[\omega_Q(t)t_p]\rangle \qquad [4]$$

is measured (*2*). If the so-called evolution time t_p is set to a small value, i.e., $\omega_Q t_p \ll 1$, the rotational correlation function of the second Legendre polynomial $f_2(t)$ will be obtained. This becomes clear by expanding the sine functions in Eq. [4] and taking into account Eq. [1],

$$F^{\sin}_{t_p}(t) \propto t_p^2\langle\omega_Q(0)\omega_Q(t)\rangle \propto f_2(t) \quad (\omega_Q t_p \ll 1). \qquad [5]$$

Consequently, the correlation time τ describing the decay of f_2 is accessible by 2D ^{2}H NMR in time domain. However, the conditions $t_p < T_2$ and $t < T_{1Q}$, the latter describing the decay of quadrupolar order, must be fulfilled to avoid a loss of signal due to relaxation.

So far, we have supposed that the evolution time t_p can be chosen sufficiently small and, thus, f_2 can be measured by applying the described three-pulse sequence, cf. Eq. [5]. In experimental practice, however, the stimulated echo disappears in the dead time of the receiver for such short evolution times t_p. Therefore, it is mandatory to insert an additional $(\pi/2)_x$ pulse after the third one in order to refocus the stimulated echo outside the dead time (*1, 14, 15*). Altogether, the following four-pulse sequence must be applied in ^{2}H NMR (*1, 14, 15*):

$$(\pi/2)_y\text{–}t_p\text{–}(\pi/4)_x\text{–}t\text{–}(\pi/4)_x\text{–}\Delta\text{–}(\pi/2)_x\text{–}t_2.$$

Still keeping the assumption of the slow motion limit, the additional pulse does not affect the results and, hence, f_2 can be measured with the displayed four-pulse sequence. We emphasize that, because of the experimental necessity for ^{2}H NMR, in all RW simulations throughout the present paper the four-pulse

sequence is taken into account. Only for a few times, which are explicitly marked, is the three-pulse sequence simulated in order to show effects arising due to the experimental application of the four-pulse sequence.

If one is not only interested in measuring f_2 but also wants to obtain further geometrical information about a molecular motion, it is useful to apply longer evolution times t_p as well. Geometrical information is obtained when varying the evolution time because t_p can be used as a geometrical filter similar to the momentum transfer Q in quasielastic neutron scattering (*11*). This meaning of t_p becomes obvious upon inspecting, once again, Eq. [4]. The longer the evolution time t_p is chosen the smaller the variation in ω_Q and, thus, the change in the molecular orientation during the mixing time t needs to be in order to cause the same loss of correlation in $F_{t_p}^{\sin}(t)$ because only the phase $\omega_Q t_p$ is relevant for the experimental result. We note that by measuring $F_{t_p}^{\sin}(t)$ for various t_p the meaning of the evolution time as geometrical filter was exploited to determine the elementary jump angles involved in the α process during the past few years (*17–20*).

Following our objective, we now drop the assumption of ultraslow motion and take into account molecular dynamics during the evolution time t_p and the echo delay Δ. This is mandatory as soon as the jump correlation time τ_j is on the order of these two delays. Of course, there are such τ_j for correlation times τ in the microsecond regime (case 3) but we emphasize that they can be found even for correlation times $\tau > T_2^*$ when looking at motions where the time scales of τ and τ_j are separated (case 2). As mentioned above, τ on the order of microseconds recently got, in principle, accessible for 2D NMR because of an extended phase cycle which allows us to set the mixing time to values $t \ll T_2^*$ (*28*). Applying this phase cycle, shorter mixing times can be used since disturbing additional signal contributions, caused by single- and double-quantum coherences which do not decay due to spin–spin relaxation during $t < T_2^*$, are suppressed. Molecular reorientations during the evolution time t_p and the echo delay Δ can be taken into account if, from the time-dependent $\omega_Q(t)$ in analogy to Eq. [2], the phases ϕ in this periods are calculated. Applying the above-displayed four-pulse sequence and evaluating the echo amplitude as usual, the following correlation function is obtained:

$$F_{t_p,\Delta}^{\sin}(t) \propto \langle \sin[\phi(0, t_p)] \sin[\phi(t', t' + \Delta) - \phi(t' + \Delta, t' + t_p + 2\Delta)] \rangle. \quad [6]$$

Here, the phases ϕ are defined according to Eq. [3] and $t' = t + t_p$ is used. Obviously, instead of the frequency ω_Q, cf. Eq. [4], different phases ϕ are now correlated. Moreover, the addition of the fourth pulse leads to an evident asymmetry of both time dimensions which is not relevant for ultraslow motions (case 1). This asymmetry in time domain is reflected by an asymmetry of the corresponding 2D NMR spectra (*29, 30*). Because of these effects it is not yet clear which information can be extracted from 2D NMR experiments in time domain if faster dynamics is studied, as found in cases 2 and 3.

Choosing different phases and pulse lengths in the described four-pulse sequence, one can also record other correlation functions (*1, 14, 15*). For example, a correlation function which is equivalent to Eq. [6] except that the two sine functions are replaced by cosine ones is measurable, too. In what follows, we will refer to these types as sin–sin and cos–cos correlation functions, respectively. We mention that, considering the latter correlation function, first, f_2 is not measured in the limit $t_p \to 0$ and, second, the signal is damped by T_1 instead of T_{1Q} during the mixing time (*1*).

2.1. Random Walk Simulations

The process of molecular reorientation is often treated in the framework of the Ivanov model (*32*), i.e., it is assumed that the orientation is constant between two rotational jumps of negligible duration. Applying such a description the molecular dynamics may be regarded as a continuous time random walk. This is the basis of RW simulations because, under these circumstances, one can mimic the stochastic process of molecular dynamics using a random number generator. More precisely, it is possible to create a large number of trajectories $\mathbf{\Omega}(t)$ describing the molecular orientation as a function of time within the scope of a certain dynamical model. Once these trajectories are known, the time dependence of the corresponding NMR frequencies and, consequently, the results of measurements can be calculated provided that the frequencies only depend on the molecular orientation (*18*). The latter requirement is met for the ^{2}H NMR experiments which are discussed here. All together, in order to calculate averages to be compared with NMR observables, RW simulations can be carried out instead of solving master equations, as has mostly been done so far (*22, 33*). As will be demonstrated, the technique of RW simulations turns out to be more flexible and easier to handle in a lot of cases.

In addition to the above-mentioned assumptions of the Ivanov model, we suppose in all simulations that the probability for a rotational jump to occur is independent of the time which has gone by since the last jump has taken place. The latter precondition will be met in RW simulations if the waiting times between two jump events are chosen from an exponential distribution (*34*), cf. below. Moreover, it is here sufficient to calculate trajectories $\theta(t)$ instead of $\mathbf{\Omega}(t)$ because axially symmetric quadrupolar coupling tensors are considered, cf. Eq. [1]. We add that, although all these assumptions are kept in the present context, they can in principle be dropped in future investigations if the technique of RW simulations is refined.

In the following, how the trajectories of the molecular orientation are simulated will be described in detail. In order to create the trajectories, dynamical models are necessary. As mentioned above, we use models reflecting molecular dynam-

ics in supercooled liquids and glasses to some extent. In particular, we take into account the following examples:

- isotropic random jump;
- isotropic rotational jump about a constant elementary jump angle γ;
- random jump on a cone with an opening angle χ;
- rotational jump on a cone with an opening angle χ involving a constant polar angle $\Delta\psi = 2\pi/n$ where n is a natural number.

Whereas the prior two models shall represent the isotropic α process, the latter two mimic the β relaxation. In addition, the first model gains some interest when studying isotropic reorientations of guest molecules in a glassy matrix (*35, 36*). In all cases, we consider exponential and nonexponential relaxation, respectively. Following Hinze (*18*), three steps are important when creating trajectories $\theta(t)$: (i) selection of a starting orientation θ_0 ensuring an isotropic distribution of $\mathbf{\Omega}_0$ as found in supercooled liquids, (ii) random choice of a waiting time from an exponential distribution characterized by the jump correlation time τ_j, and (iii) calculation of the new orientation after the jump. After step (i), steps (ii) and (iii) are alternately repeated until a trajectory of sufficient length is recorded where the length is determined by the duration of a single-shot experiment.

The geometry of the above-listed dynamical model comes into play in step (iii). When simulating an isotropic random jump, according to the definition of this kind of motion, the new orientation after a jump is always chosen randomly as it is in step (i). Assuming an isotropic $\gamma°$ jump, the orientation θ_{i+1} after the jump can be calculated from the one before θ_i using (*18*)

$$\theta_{i+1} = \arccos[\sin\theta_i \sin\gamma\cos\psi + \cos\theta_i\cos\gamma], \qquad [7]$$

where ψ is taken from the interval $[0, 2\pi[$ with equal probability. In the case of reorientations on a cone with opening angle χ, the orientation of the cone axis θ_a is chosen by chance at the beginning of each trajectory, ensuring an isotropic distribution of all axes. Afterward, the starting orientation as well as all other positions throughout a trajectory are calculated according to Eq. [7] with fixed $\theta_i = \theta_a$ and $\gamma = \chi/2$. Depending on the model, ψ is either selected randomly from the interval $[0, 2\pi[$ or varied by $\Delta\psi$ each time.

The time scale of the dynamics within one of these models is adjustable by the choice of the jump correlation time τ_j. When investigating random jumps the correlation time τ equals the jump correlation time τ_j because the maximal loss of correlation is achieved with each reorientation. On the other hand, in the case of an isotropic $\gamma°$ jump, several elementary rotational jumps are necessary to destroy the correlation. This leads to the above-mentioned separation of the time scales of τ and τ_j which is quantified by the expression (*37*)

$$\frac{\tau_j}{\tau} = \frac{3}{2}\sin^2\gamma. \qquad [8]$$

It becomes clear that the elementary jumps will take place on a completely different time scale than the loss of correlation if γ is small. When simulating nonexponential relaxation, a heterogeneous distribution of correlation times $G(\lg\tau)$ can be taken into account by using different τ_j for the various trajectories but keeping τ_j fixed during the course of one individual $\theta(t)$.

Having recorded the trajectories $\theta(t)$ it is a straightforward task to obtain the corresponding results of 1D ^{2}H NMR spectra and of 2D ^{2}H NMR experiments in time domain. First, the time dependence of $\omega_Q(t)$ is determined according to Eq. [1] where $\delta = 2\pi \times 125$ kHz is used in all simulations. Afterward, the time signals during the solid-echo sequence and the above-mentioned four-pulse sequences are calculated using Eqs. [2] and [6], respectively. The phases ϕ appearing in these equations, cf. Eq. [3], are evaluated as sum over the different phase shifts which are achieved during the various periods of constant frequency, i.e., during the waiting times. Finally, calculating results of 2D experiments, the amplitude of the stimulated echo for various mixing times t is evaluated as it is in a real measurement. On the other hand, the 1D spectra are obtained after a FT of the time signal during the solid-echo sequence starting at $t = 2t_p$.

So far, we assumed ideal experimental conditions. However, several additional effects appear in real experiments which, therefore, must be regarded at this point. Calculating 1D spectra, first, one has to take into account the line broadening due to static dipole–dipole interaction. This is done in the RW simulations by damping the time signal with a gaussian function before carrying out the FT. Further, the finite pulse lengths in a real measurement have to be considered. Following Bloom *et al.* (*38*), this is achieved by multiplying the obtained spectra with a function $A(\omega_Q)$ which describes the excitation effect arising for finite pulse lengths,

$$A(\omega_Q) = \omega_p\Delta_p \frac{\sin(\Delta_p\sqrt{\omega_p^2 + \tfrac{1}{2}\omega_Q^2})}{\Delta_p\sqrt{\omega_p^2 + \tfrac{1}{4}\omega_Q^2}}. \qquad [9]$$

In this equation, Δ_p is length of a $(\pi/2)$-pulse and ω_p represents the angular velocity of the rotation imposed on the magnetization by this pulse. In all simulations, the various parameters describing damping and excitation effect are kept fixed. They are chosen in such a way that 1D spectra similar to experimental ones result as will be described in detail elsewhere (*21*). For example, $\Delta_p = 3.8\ \mu$s is used in all simulations. Since dipole–dipole interaction and finite excitation bandwidth of the pulse irradiation are expected to have little influence on 2D ^{2}H NMR experiments in time domain for the chosen dynamical models, both effects are neglected when calculating sin–sin and cos–

cos correlation functions, respectively. Furthermore, we do not take into account molecular dynamics during the RF pulses in any of our RW simulations.

3. RESULTS AND DISCUSSION

In what follows, we present the results of various RW simulations. We begin by discussing the findings for 2D ^{2}H NMR in time domain and will later describe the observations for 1D ^{2}H NMR spectra.

3.1. 2D NMR in Time Domain

As aforementioned, dealing with 2D ^{2}H NMR in time domain we mainly address three questions. First, we investigate whether it is possible to measure the correlation function f_2 even for correlation times $\tau < T_2^*$, i.e., for τ on the order of microseconds. Then, we study how 2D NMR experiments in time domain are affected by highly restricted motions and, finally, we look at the influence of very broad distributions $G(\lg\tau)$. However, before tackling these problems we would like to insert some comments on the proceeding.

In order to parametrize the simulated sin–sin and cos–cos correlation functions (i = sin, cos), a suitably modified Kohlrausch–Williams–Watts (KWW) function (*39, 40*)

$$F^i_{t_p}(t) = (1 - C^i_{t_p})\exp\left(-\left(\frac{t}{\tau^{\text{app}}_{t_p}}\right)^{\beta_{t_p}}\right) + C^i_{t_p}, \qquad [10]$$

is fitted to the data as is usually done when analyzing measurements in supercooled liquids (*17–20*). This function allows us to characterize the time scale $\tau^{\text{app}}_{t_p}$ and the stretching β_{t_p} for exponential and nonexponential decays, respectively. The index t_p is used in Eq. [10] since the measured decay depends on the applied evolution time, cf. Eq. [6]. The superscript "app" shall indicate that the time constant $\tau^{\text{app}}_{t_p}$ is the correlation time which one would apparently measure in a real experiment provided that there is the same kind of dynamics as in the simulation. Furthermore, introducing a rest correlation $C^i_{t_p}$, an incomplete loss of correlation, e.g., in the case of restricted dynamics, can be taken into account. Assuming the slow motion limit an evaluation of the rest correlation $C^i_{t_p}$ as a function of the evolution time reveals information of the geometry of the considered molecular dynamics (*11*). We note in passing that the KWW function is solely used as a fitting function in the present context but is not thought to have any physical meaning. Fitting an exponential decay with Eq. [10] β_{t_p}, of course, equals 1 and $\tau^{\text{app}}_{t_p}$ directly represents the time constant of the loss of correlation. In contrast, assuming a distribution $G(\lg\tau)$, the resulting nonexponential decay leads to a $\beta_{t_p} < 1$. Then, the apparently measured mean correlation time can be calculated according to (*17*),

$$\langle\tau^{\text{app}}_{t_p}\rangle = \frac{\tau^{\text{app}}_{t_p}}{\beta_{t_p}}\,\Gamma(1/\beta_{t_p}), \qquad [11]$$

where Γ denotes the gamma function.

When intending to mimic a real measurement of the correlation function f_2 we have to use a short evolution time t_p in the RW simulations, cf. Eq. [5]. Here, we apply $t_p = 3\ \mu$s throughout the paper where this particular value is motivated by the observation that shorter effective evolution times are hardly accessible in real 2D ^{2}H NMR experiments. This comes about due to both the finite pulse lengths (*19*) and the decrease of the signal amplitude ($\propto t_p^2$) for $t_p \to 0$, cf. Eq. [5]. For the echo delay in the four-pulse sequence, we apply a typical experimental value $\Delta = 15\ \mu$s. Finally, we add that we will skip the index t_p when considering f_2, i.e., if according to our proceeding sin–sin correlation functions with $t_p = 3\ \mu$s are simulated.

3.1.1. Isotropic dynamics: Exponential relaxation. Using various dynamical models we now want to analyze whether one can measure f_2 for τ in the microsecond regime. First, we simulate an isotropic random jump assuming exponential relaxation. According to our goal, we study the sin–sin correlation functions ($t_p = 3\ \mu$s) for various jump correlation times τ_j covering the range from some microseconds to the millisecond regime. Strictly speaking, the amplitude of the stimulated echo after the four-pulse sequence ($\Delta = 15\ \mu$s) is calculated for various mixing times t using Eq. [6]. The results together with fits obtained by applying Eq. [10] ($\beta_{t_p} = 1$) are displayed in Fig. 1a. Looking at the fit parameter τ^{app}, which is expected to represent the correlation time τ measured in an experiment, it becomes evident that, for all jump correlation times used in the simulation, $\tau_j = \tau^{\text{app}}$ holds within an error of about 1%. This error is caused by the noise in the RW simulation due the finite number of trajectories ($N = 50{,}000$). The good agreement of τ^{app} and τ is, on the one hand, a consequence of the random jump mechanism because, in this case, the correlation time τ equals the jump correlation time τ_j and, on the other hand, this finding demonstrates that even for dynamics on the time scale of about 10 μs correct correlation times can be measured within the scope of the applied model.

However, the amplitude of the measurable signal, i.e., the signal for $t \ll \tau$, declines when leaving the slow motion limit and considering faster dynamics. This decrease is caused by molecular dynamics taking place during the evolution time t_p and the echo delay Δ. In a RW simulation, the dependence of the measurable signal on the correlation time can be characterized by the reduction factor $R^{\text{2D}}_{t_p,\Delta}(\tau)$. In analogy to the well-known reduction factor of 1D NMR, we define this quantity in the present context as the amplitude of the stimulated echo resulting for $t = 0$ and a certain τ divided by the height for $\tau \to \infty$. Of course, the same number of trajectories must be accumulated for all τ. The reduction factor $R^{\text{2D}}_{3,15}(\tau)$ for the isotropic random jump is displayed in Fig. 1b. For comparison, we have also included the reduction factor for $\Delta = 100\ \mu$s and

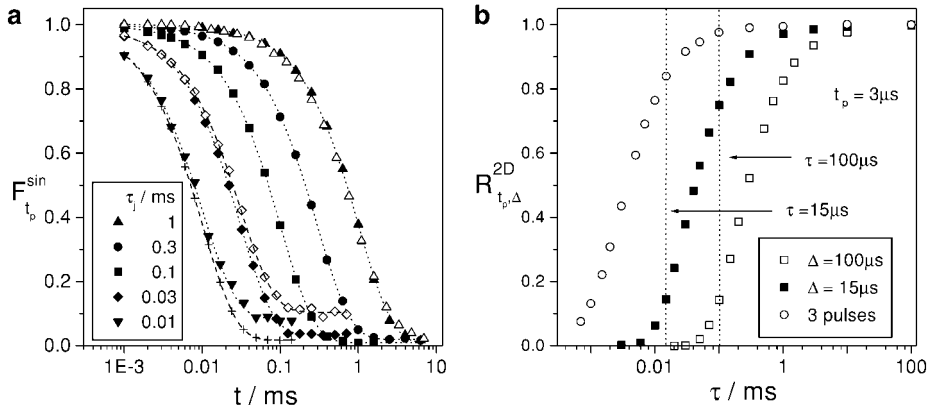

FIG. 1. RW simulations for the models of an isotropic random jump and an isotropic 15° jump: (a) sin–sin correlation functions; solid symbols: isotropic random jump (four-pulse sequence: $t_p = 3$ μs, $\Delta = 15$ μs), open symbols: isotropic 15° jump (four-pulse sequence: $t_p = 3$ μs, $\Delta = 15$ μs), crosses: isotropic random jump (three-pulse sequence: $t_p = 3$ μs, $\tau_j = 10$ μs), dotted and dashed lines: fits using Eq. [10], inset: jump correlation times τ_j for the random jump; (b) reduction factors of the stimulated echo for the model of an isotropic random jump: $R^{2D}_{t_p,\Delta}(\tau)$ (four-pulse sequence: $t_p = 3$ μs and $\Delta = 15$ μs, 100 μs) and analogous defined reduction factor for the three-pulse sequence ($t_p = 3$ μs).

for the three-pulse sequence ($t_p = 3$ μs) assuming the same kind of motion. It is evident that the amplitude of the signal strongly decreases with declining τ in all cases. However, a dependence of the reduction factor on the applied pulse delays becomes obvious as well. Considering the four-pulse sequence the echo amplitude starts to decrease at $\tau \approx 10\Delta$, whereas looking at the three-pulse sequence an inset of the decline is visible at $\tau \approx 10t_p$. Finally, for $\tau < \Delta$ and $\tau < t_p$, respectively, a signal is hardly measurable any longer. These findings demonstrate that the longest delay of the applied pulse sequence determines the reduction factor which, of course, is a plausible result. Therefore, having in mind that in real experiments the four-pulse sequence with an echo delay $\Delta \approx 15$ μs is applied, correlation times shorter than $\tau \approx 10$ μs, say, cannot be determined by applying 2D ^{2}H NMR and even for $\tau < 1$ ms, the number of scans carried out in the experiment has to be increased in order to obtain a sufficiently large signal-to-noise ratio. We already note that these observations will gain some importance if a distribution of correlation times $G(\lg\tau)$ is present. Further, we add that a similar behavior of the reduction factor is found recording 1D (*3*, *5*, *7*) and 2D ^{2}H NMR spectra (*29*, *30*). This is reasonable because, in these experiments, echo techniques are used as well.

Inspecting once again Fig. 1a, still another effect is visible. The final state value of $F^{\sin}_{t_p}(t)$ for $t \gg \tau$, which is characterized by the fit parameter $C^{\sin}_{t_p}$, cf. Eq. [10], does not only depend on t_p, as found for ultraslow motion, but also on τ. Referring to the decay curves in Fig. 1a, this parameter increases from about 1% in the slow motion limit, which is in accordance with the theoretical value for an isotropic motion (*11*), to about 9% for $\tau = 10$ μs. The increased value of $C^{\sin}_{t_p}$ for short τ again arises because of motion during the various dephasing and refocusing periods in the experiment. When simulating f_2 the enhanced value mainly comes up because of dynamics during the echo delay $\Delta > t_p$. This can be shown in the simulation by reducing Δ in the four-pulse sequence or by calculating the correlation function f_2 after the three-pulse sequence which cannot be measured. The latter is included in Fig. 1a as well. Obviously, using $\tau = 10$ μs, the increase of $C^{\sin}_{t_p}$ disappears for the three-pulse sequence. The growth of $C^{\sin}_{t_p}$ for $\tau \approx \Delta$ is plausible since such kind of dynamics leads to an exchange in the frequency during the period Δ and, thus, to an "average" over a few $\omega_Q(t)$ when calculating the phase of the second sine function in Eq. [6]. Therefore, with respect to a certain $\omega_Q(0)$, the maximal loss of correlation cannot be reached. These findings demonstrate that the enhanced final state value of $F^{\sin}_{t_p}(t)$ arising for $\tau \approx \Delta$ is an artifact caused by the experimental application of the four-pulse sequence.

Very similar observations are found if an exponential relaxation caused by an isotropic 15° jump is simulated. In particular, over the whole range of correlation times $\tau > 10$ μs, correct time constants can be measured for this motion as well. This is again demonstrated in Fig. 1a where the open symbols mark the RW simulations for the isotropic 15° jump and the dashed lines mark the corresponding fits to Eq. [10]. Using jump correlation times $\tau_j = 3$ μs and $\tau_j = 100$ μs in the simulation, respectively, correlation times $\tau^{app} = 30$ μs and $\tau^{app} = 1$ ms are obtained from the fits. Hence, in both cases $\tau^{app} = 10\tau_j$ holds as is expected according to Eq. [8] and, thus, a proper time constant is available. However, considering the 15° jump the increase of $C^{\sin}_{t_p}$ for $\tau \approx \Delta$ is even more pronounced than in the case of the random jump. This is clearly seen when comparing the decays corresponding to $\tau^{app} = 30$ μs for both models in Fig. 1a. The observation is understood if one takes into account that for the 15° jump, due to the shorter τ_j, more reorientations take place during the period Δ.

We add that the described effects were also observed in an experimental investigation of an anisotropic motion. Studying the sixfold jump of the molecules in crystalline hexamethylbenzene correct correlation times in the microsecond regime

could be measured by applying 2D ^{2}H NMR in time domain (*21*, *41*). Moreover, when looking at $\tau < T_2^*$ a larger value of $C_{t_p}^{\sin}$ was found than in the slow motion limit.

We conclude that it is possible to extract correlation times 10 $\mu s \leq \tau \leq T_{1Q}$ from 2D ^{2}H NMR experiments in time domain if exponential relaxation is considered which involves isotropic motions or anisotropic large angle reorientations, respectively. Consequently, the time window of this 2D experiment can be enlarged by approximately 2 decades when looking at such dynamics and applying an extended phase cycle (*28*). However, care must be taken if the rest correlation $C_{t_p}^{\sin}$ is evaluated to analyze the geometry of a motion characterized by a correlation time $\tau \approx \Delta$.

3.1.2. Isotropic dynamics: Nonexponential relaxation. Now, we consider a distribution of correlation times $G(\lg\tau)$. In this case, the resulting nonexponential correlation function f_2 can be measured by applying 2D NMR in time domain if for all τ out of this distribution the slow motion limit holds (case 1). Here, we check whether this is still true when parts of the distribution enter the regime $\tau < T_2^*$. We assume a heterogeneous logarithmic Gaussian distribution

$$G(\lg\tau) = \frac{1}{\sqrt{2\pi\sigma^2}} \exp\left(- \frac{(\lg\tau - \lg\tau^{\mathrm{m}})^2}{2\sigma^2} \right). \qquad [12]$$

Using such a $G(\lg\tau)$ the mean logarithmic correlation time $\langle \lg\tau \rangle$ equals the maximum of the distribution $\lg\tau^{\mathrm{m}}$ and the decadic full width at half maximum of $G(\lg\tau)$ is given by $2\sigma\sqrt{2 \ln 2}$. In all RW simulations concerning nonexponential isotropic dynamics, we choose $\sigma = 0.8$ corresponding to a distribution with a half width of about 1.9 decades, which is typical of the α process in supercooled liquids.

First, we study an isotropic random jump in the presence of such a distribution $G(\lg\tau)$. Following our objective we calculate sin–sin correlation functions varying $\lg\tau^{\mathrm{m}}$. The results, using again $t_p = 3$ μs and $\Delta = 15$ μs, are compiled in Fig. 2. Although only a poor interpolation is reached, the data are fitted to Eq. [10] in order to characterize time scale and stretching of the decays as was done in prior work (*17–20*). The systematic deviations occur because, on the one hand, a logarithmic Gaussian distribution $G(\lg\tau)$ is used in the simulation and, on the other, a fit to a KWW function is applied. Nevertheless, we want to disregard these problems because no quantitative results are to be obtained but only trends shall be shown. Inspecting Fig. 2, two effects are obvious when $\lg\tau^{\mathrm{m}}$ is decreased with constant increment: First, the sin–sin correlation functions become less nonexponential and, second, they are less shifted to smaller values for small τ^{m}.

These effects can be quantified displaying both the fit parameter β_{t_p} and the mean time constant $\langle \tau^{\mathrm{app}} \rangle$, which is obtained from $\tau_{t_p}^{\mathrm{app}}$ and β_{t_p} according to Eq. [11], as a function of τ^{m} in Fig. 3. Strictly speaking, in the latter case, the dependence of the ratio $\langle \tau^{\mathrm{app}} \rangle / \tau^{\mathrm{m}}$ on τ^{m} is shown in Fig. 3a. For the ratio, a

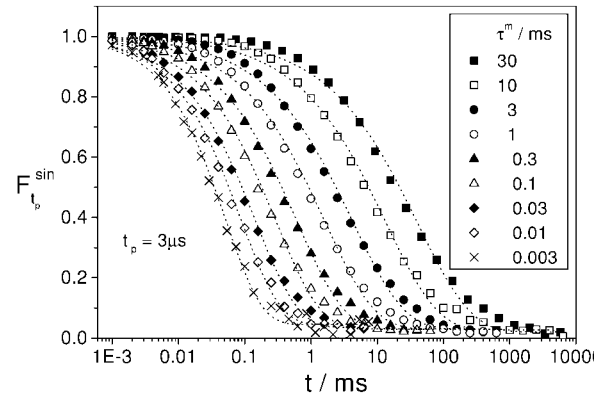

FIG. 2. RW simulations for the model of an isotropic random jump assuming a logarithmic gaussian distribution $G(\lg\tau)$ ($\sigma = 0.8$), cf. Eq. [12]: sin–sin correlation functions for various mean logarithmic correlation times $\lg\tau^{\mathrm{m}}$ (four-pulse sequence: $t_p = 3$ μs, $\Delta = 15$ μs). Dotted lines: fits using Eq. [10].

horizontal line will be expected if the measured mean time constant $\langle \tau^{\mathrm{app}} \rangle$ varies according to the shift of the distribution $G(\lg\tau)$. Indeed, such a behavior is found for ultraslow motion. However, if $G(\lg\tau)$ contains $\tau < T_2^*$, this is no longer true and the ratio increases, i.e., the apparently measured time constant $\langle \tau^{\mathrm{app}} \rangle$ is too long. We mention in passing that even in the slow motion limit $\langle \tau^{\mathrm{app}} \rangle$ should not equal τ^{m} because different averages are regarded. Concerning β_{t_p} an increase from 0.54 to 0.79 is visible in Fig. 3b, indicating the less nonexponential loss for small τ^{m}.

Both observations can be explained, remembering that magnetization of molecules with correlation times $\tau < T_2^*$ is not completely refocused in the four-pulse sequence, cf. Fig. 1b. This finding means that only as long as $G(\lg\tau)$ solely contains τ in the slow motion limit, all parts of the distribution uniformly contribute to the experimental result. However, this is no longer valid when parts of $G(\lg\tau)$ enter the microsecond regime. Then, shorter τ contribute less to the echo, as is seen in the declining reduction factor $R_{3,15}^{\mathrm{2D}}(\tau^{\mathrm{m}})$, cf. Fig. 3c. Consequently, the findings are no longer determined by the real distribution $G(\lg\tau)$ but by an effective distribution $G^*(\lg\tau)$ which is obtained by a multiplication of $G(\lg\tau)$ with the reduction factor $R_{3,15}^{\mathrm{2D}}(\tau)$, cf. Fig. 1b, since the latter quantity describes the reduced signal contribution for short τ. The distribution $G^*(\lg\tau)$ is the narrower the smaller τ^{m} because the portion which is cut off by $R_{3,15}^{\mathrm{2D}}(\tau)$ becomes larger and larger when reducing τ^{m}. Hence, a less nonexponential correlation function and an increase of β_{t_p} with decreasing τ^{m} result in agreement with the observations. Moreover, since the "fast part" of the real distribution contributes to $G^*(\lg\tau)$ only in a reduced manner, correlation times τ in the slow motion limit are overestimated in the measured average $\langle \tau^{\mathrm{app}} \rangle$ and, thus, $\langle \tau^{\mathrm{app}} \rangle$ is longer than one would expect considering the real distribution $G(\lg\tau)$. As a consequence, the ratio $\langle \tau^{\mathrm{app}} \rangle / \tau^{\mathrm{m}}$ grows with declining τ^{m}. We add that all these effects also appear if

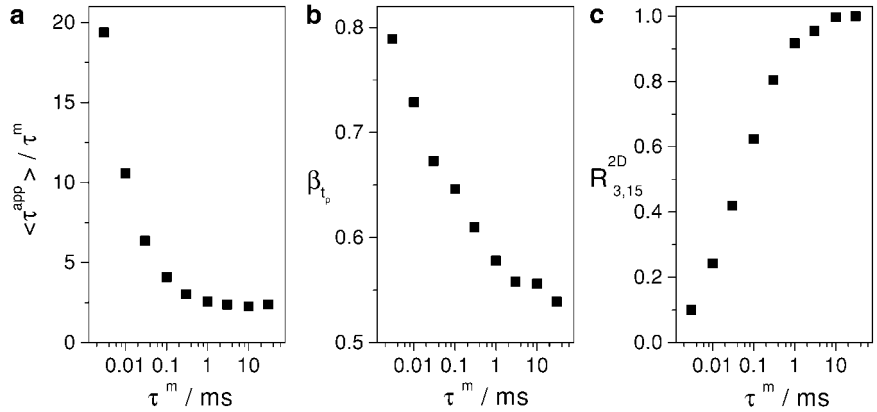

FIG. 3. Parameters obtained from fitting the data in Fig. 2 to Eq. [10]: (a) Ratio $\langle\tau^{app}\rangle/\tau^{m}$; (b) stretching parameter τ_{t_p}; and (c) reduction factor $R^{2D}_{t_p,\Delta}(\tau^{m})$.

an isotropic rotational jump involving a constant jump angle γ is studied as has been checked by carrying out some simulations for that model.

Summarizing, it has turned out that the correlation function f_2 is not correctly measured by applying 2D ^{2}H NMR in time domain if there is a distribution $G(\lg\tau)$ which contains τ in the microsecond regime. In this case, the different parts of the distribution do not contribute uniformly to the signal and too long time constants $\langle\tau^{app}\rangle$ are obtained.

3.1.3. Restricted dynamics: Exponential relaxation. Next, we turn to highly restricted dynamics. As mentioned above, these investigations are relevant for a forthcoming analysis of experimental results on the β process in supercooled liquids and glasses (*21*). In what follows, we try to make such restricted motions visible by applying 2D ^{2}H NMR in time domain. For that purpose, we simulate cos–cos correlation functions assuming reorientations on a cone. The cos–cos instead of the sin–sin correlation functions are now calculated since, for experimental reasons concerning spin–lattice relaxation during the mixing time (*19, 21*), they were considered in our study of the β process. The opening angle of the cone is set to $\chi = 6°$ in all RW simulations where this particular value is motivated by our experimental findings (*21, 42*). Moreover, the model of reorientations on a cone is chosen because, on the one hand, it is more flexible than a two-site jump, for example, various jump angles $\Delta\psi$ on the cone can be implemented and, on the other, it is still easy to simulate.

First, we calculate cos–cos correlation functions ($\Delta = 15$ μs) for the model of a random jump on the cone where the jump correlation time τ_j amounts to 10 ms. This means we study ultraslow motion to circumvent the above-discussed problems arising in the presence of faster dynamics for the moment. The data for various evolution times t_p together with fits according to Eq. [10] ($\beta_{t_p} = 1$) are compiled in Fig. 4. It is obvious that, independent of t_p, the time constants of the different decays $\tau^{app}_{t_p}$ well agree with the jump correlation time $\tau_j = 10$ ms as is expected for a random jump. On the other hand, the amount of correlation remaining for $t \gg \tau_j$ which is reflected by the fit parameter $C^{cos}_{t_p}$ strongly depends on the evolution time. Almost no loss of correlation can be observed for $t_p \leq 5$ μs whereas a distinct decay appears for larger evolution times. Especially, in the range 5 μs $< t_p <$ 55 μs, $C^{cos}_{t_p}$ clearly decreases with an extension of the evolution time. Finally, if one applies $t_p > 55$ μs the cos–cos correlation functions are less affected by a similar variation of this delay. We note that the observed dependence of the rest correlation $C^{cos}_{t_p}$ on t_p is completely different from the one found for isotropic dynamics (*11*). However, a qualitatively similar dependence of the rest correlation on t_p was reported for the model of rotational diffusion on a cone with $\chi = 60°$ when considering sin–sin correlation functions (*13*). Quantitatively, of course, much smaller absolute values of the rest correlation were found for a cone with opening angle $\chi = 60°$ than for the one with $\chi = 6°$ in the present context. Furthermore, we add that we have also calculated the correlation function f_2, i.e., the sin–sin correlation function for $t_p = 3$ μs, using the model of a random jump on a cone with an opening angle of $\chi = 6°$. Like the cos–cos correlation function for a short evolution time $t_p = 5$ μs in Fig. 4, f_2 exhibits no discernible loss. Therefore,

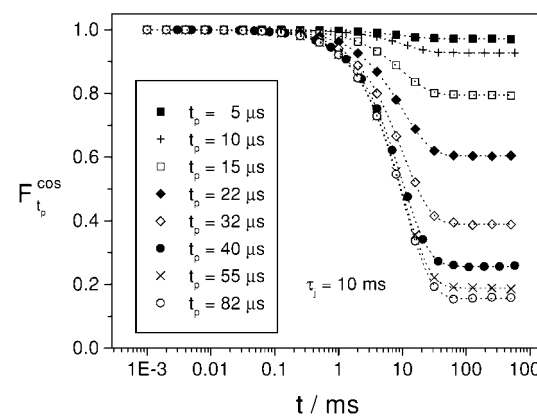

FIG. 4. RW simulations for the model of a random jump on a cone ($\chi = 6°$): cos–cos correlation functions for $\tau_j = 10$ ms and various evolution times t_p (four pulse sequence: $\Delta = 15$ μs). Dotted lines: fits using Eq. [10].

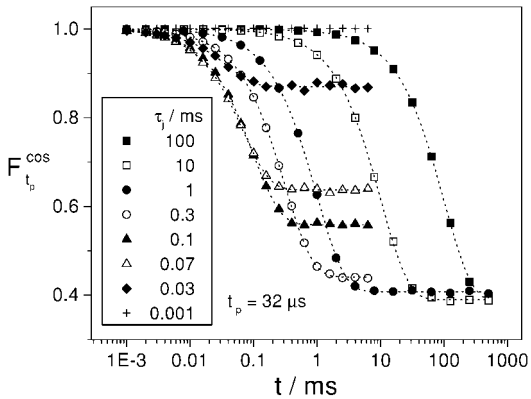

FIG. 5. RW simulations for the model of a random jump on a cone (χ = 6°): cos–cos correlation functions for different τ_j (four-pulse sequence: Δ = 15 μs, t_p = 32 μs). Dotted lines: fits using Eq. [10].

in experimental practice, it is very difficult to determine the correlation times τ of highly restricted reorientations in general.

The dependence of $C_{t_p}^{cos}$ on the evolution time, displayed in Fig. 4, is understood if the filter effect of t_p is taken into account, cf. Eq. [4]. Investigating highly restricted motions only small changes in frequency, typically $\Delta\omega_Q$, say, can occur during the mixing time. If short t_p are chosen, these changes do not cause a detectable loss of correlation because the phases before and after the mixing time differ only a little by $\Delta\omega_Q t_p \ll 1$. However, increasing t_p leads to larger differences in the phases even for such small $\Delta\omega_Q$ and, therefore, a significant decay of the correlation functions can be observed.

Now, we look at what happens when the slow motion limit is left but sufficiently large t_p are applied in order to make the loss of correlation visible. Therefore, we calculate cos–cos correlation functions for a constant t_p = 32 μs but different τ_j, applying once again the model of a random jump on the cone. The results and the fits according to Eq. [10] (β_{t_p} = 1) are compiled in Fig. 5. It turns out that, for all $\tau_j \geq 30$ μs, the fits yield time constants $\tau_{t_p}^{app}$ which are in good agreement with the jump correlation time. However, in comparison with the results obtained for an isotropic random jump and a evolution time t_p = 3 μs, cf. Fig. 1a, the dependence of the rest correlation $C_{t_p}^{cos}$ on τ is much stronger. Above all, reducing τ_j from 300 to 30 μs leads to a strong increase of $C_{t_p}^{cos}$. For even shorter τ_j, no decay is visible any longer. These observations are plausible having in mind that, during the necessarily longer evolution time t_p for restricted motions, the effects of molecular dynamics in this period are amplified. We note that the described findings gain some relevance if a distribution $G(\lg\tau)$ is present as discussed below.

All together, highly restricted dynamics can clearly be observed in 2D NMR experiments in time domain if large evolution times t_p are applied. However, considering such small angle fluctuations it is difficult to determine the correlation time τ in general.

3.1.4. Restricted dynamics: Nonexponential relaxation. Finally, we introduce a distribution $G(\lg\tau)$ for highly restricted motions, too. In particular, we deal with very broad distributions typical of the β process in supercooled liquids and glasses. As will be shown, when shifting such a $G(\lg\tau)$ through the time window of 2D NMR in time domain peculiar results appear in the RW simulations which are similar to experimental findings to be presented elsewhere (*21*).

Once again, we consider a random jump on the cone. Now, however, we assume a very broad logarithmic Gaussian distribution $G(\lg\tau)$ characterized by σ = 2.3, cf. Eq. [12]. In this case, the corresponding full width at half maximum of 5.4 decades represents a typical value for distributions describing the β process near the liquid to glass transition (*27*). According to the experimental procedure where various temperatures are considered, we simulate cos–cos correlation functions varying $\lg\tau^m$ and keeping t_p = 32 μs fixed. As has been demonstrated for exponential relaxation, such large evolution times are necessary to obtain a discernible decay of the correlation functions, cf. Fig. 4. Again, the four-pulse sequence with an echo delay Δ set to 15 μs is taken into account. The results are shown in Fig. 6, however, the displayed data are further damped by an exponential decay with a time constant equal to 1 s. This additional damping is introduced in order to reflect approximately the experimental situation where the amplitude of the stimulated echo is reduced by spin–lattice relaxation and by spin diffusion for long mixing times. As will become clear below, the additional damping is necessary to allow a demonstration of effects appearing in experiments for very broad distributions $G(\lg\tau)$. Because of our proceeding, the resulting data in Fig. 6 show two decays: first, a strongly stretched short time decay caused by the loss of orientational correlation due to the considered motion and, second, an exponential long time decay because of the applied damping. Inspecting the short

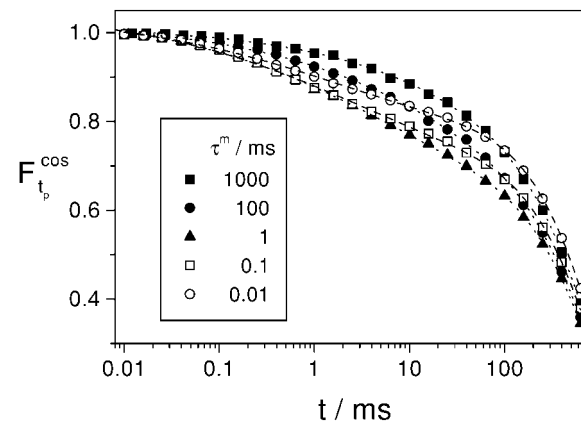

FIG. 6. RW simulations for the model of a random jump on a cone (χ = 6°) assuming a very broad logarithmic gaussian distribution $G(\lg\tau)$ (σ = 2.3), cf. Eq. [12]: cos–cos correlation functions for different mean logarithmic correlation times $\lg\tau^m$ (four-pulse sequence: Δ = 15 μs, t_p = 30 μs). Dotted lines: fits described in the text. The calculated data are damped by an exponential decay with a time constant of 1 s.

time decay, a peculiar behavior becomes evident. Although τ^{m} is varied by 5 orders of magnitude no clear shift of the correlation function is visible. This is seen, for example, comparing the data for $\tau^{m} = 100$ ms and $\tau^{m} = 10$ μs, respectively. Furthermore, the amount of correlation that is lost until the long time decay becomes effective at $\tau \approx 100$ ms exhibits a maximum using $\tau^{m} = 1$ ms. For both shorter and longer τ^{m} the observable loss of correlation is less pronounced.

These qualitative observations can be quantified by fitting the data to a KWW function, cf. Eq. [10], multiplied with an additional exponential decay. The time constant of this exponential decay T_{damp}, although known in the simulation, is varied in the fitting procedure, too, in order to mimic the experimental situation. Nevertheless, for all curves, $T_{damp} \approx 1$ s is obtained from the fits in accordance with the used damping. Concerning the stretching parameter of the short time decay β_{t_p}, independent of τ^{m}, small values of 0.34 ± 0.01 are found due to the broad distribution $G(\lg\tau)$. The time constant of this decay $\tau_{t_p}^{app}$ is reduced from about 35 ms for $\tau^{m} = 1$ s to about 1.3 ms for $\tau^{m} = 10$ μs. Thus, as already expected, a decrease of τ^{m} by 5 orders of magnitude causes only a variation in $\tau_{t_p}^{app}$ by a factor of 30. Therefore, applying 2D NMR in time domain and considering such broad $G(\lg\tau)$ it is impossible to extract correct correlation times. Instead, the measured time constant is fixed by the time window of the experiment and, hence, on the order of a few milliseconds.

Nevertheless, information about the position of a broad $G(\lg\tau)$ is available evaluating $(1 - C_{t_p}^{cos})$ as will now be demonstrated. For that purpose, we look at the amount of correlation that is lost in the time window of 2D experiments when investigating such a distribution. On the one hand, fitting the data the amount of loss is expected to be reflected by $(1 - C_{t_p}^{cos})$, on the other hand, it is supposed to depend on the number of molecules relaxing, i.e., on the part of the broad distribution $G(\lg\tau)$ located in the experimental time window. Therefore, comparing both quantities as a function of τ^{m} perhaps a similar behavior should be found. If this were true a determination of $(1 - C_{t_p}^{cos})$, using experimental data, indeed, would yield information about an unknown distribution. In order to check our speculations, we have to estimate the time window of our particular 2D experiment first. Toward long τ, it is limited by the long time decay imitating spin–lattice relaxation. This decrease starts to dominate the decline of the stimulated echo at $t \approx 100$ ms, cf. Fig. 6. The lower boundary is about 100 μs. Using an evolution time $t_p = 32$ μs this approximation seems to be reasonable because for $\tau < 100$ μs; first, there is only a slight decay of the correlation functions, cf. Fig. 5, and, second, the contribution of such τ to the measured signal is smaller due to the incomplete refocusing of the corresponding magnetization, cf. also Fig. 1b. All together, the loss of correlation detected in the 2D experiment should be connected with the integral

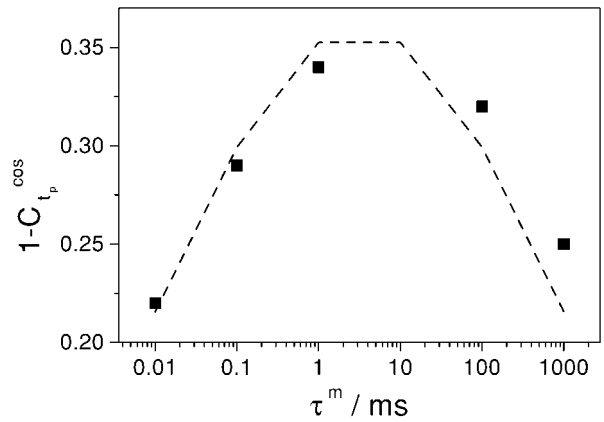

FIG. 7. Parameter $(1 - C_{t_p}^{cos})$ obtained from fitting the data in Fig. 7. Dotted line: value of the integral in Eq. [13] for various $\lg\tau^{m}$.

$$(1 - C_{t_p}^{cos}) \propto \int_{\lg 100\ \mu s}^{\lg 100\ ms} G(\lg\tau)\, d\lg\tau. \qquad [13]$$

The values of this integral for several τ^{m} and the fit parameters $(1 - C_{t_p}^{cos})$ are shown in Fig. 7, respectively. As expected, a good agreement is evident. In particular, both curves exhibit a maximum at $\tau^{m} \approx 1$ ms which has been anticipated in the first inspection of the data as well. Slight differences occur due to the rough estimation of the integration limits. These findings demonstrate that the quantity $(1 - C_{t_p}^{cos})$ is not only determined by the geometry of a motion (*11*), but also correlated with the number of molecules relaxing in the time window of 2D NMR in time domain. Therefore, if the shape of $G(\lg\tau)$ is approximately known a determination of $(1 - C_{t_p}^{cos})$ as a function of temperature allows us to estimate the mean correlation time by carrying out 2D NMR experiments.

It has turned out that it is impossible to measure the mean correlation time directly by applying 2D NMR in time domain if an extremely broad distribution $G(\lg\tau)$ is present. However, evaluating $(1 - C_{t_p}^{cos})$ yields at least a clue to the position of $G(\lg\tau)$. This result, explicitly demonstrated for highly restricted motions, is expected to hold generally for distributions broader than the experimental time window. Such broad distributions appear, e.g., when investigating the β process in supercooled liquids (*27*) or the reorientation of guest molecules in glasses (*35*, *36*).

3.2. 1D NMR Spectra

In the remaining part of this paper, we carry out RW simulations to calculate 1D ^{2}H NMR spectra for different dynamical models. In all simulations, the solid-echo pulse sequence with an echo delay t_p is considered. Again, isotropic as well as highly restricted motions are taken into account but, here, exponential relaxation is solely discussed. In particular, complex molecular dynamics characterized by two different time

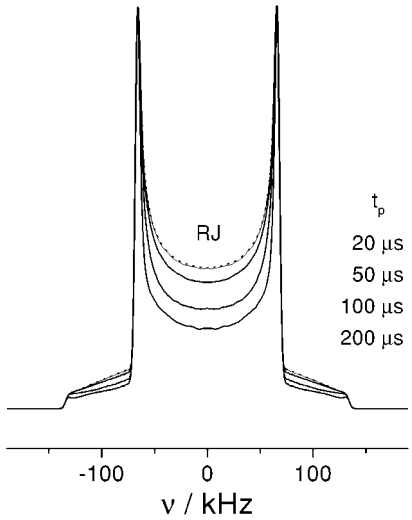

FIG. 8. RW simulations for the model of an isotropic 3° jump (τ = 100 ms, τ_j = 411 μs): 1D ^{2}H NMR spectra for different echo delays t_p in the solid-echo sequence. Dotted line: 1D ^{2}H NMR spectrum for an isotropic random jump ($\tau = \tau_j$ = 100 ms) and an echo delay t_p = 200 μs.

constants $\tau_j < T_2^*$ and $\tau > T_2^*$ is investigated, i.e., case 2 is regarded. As mentioned above, we mainly follow the question of whether such dynamics, which is usually analyzed by applying multidimensional NMR techniques, can simultaneously be studied by recording 1D spectra. If this were true, additional information about the motion would be available since any dynamical model has to reproduce the results of 1D and 2D NMR experiments at the same time.

3.2.1. Isotropic dynamics: Exponential relaxation. In order to obtain well-separated time constants $\tau_j < T_2^* < \tau$ we now consider an isotropic 3° jump. Using this model the jump correlation time τ_j is by a factor of about 240 shorter than the correlation time τ, cf. Eq. [8]. We calculate solid-echo spectra varying both τ and the echo delay t_p. First, we keep the correlation time fixed at a value τ = 100 ms, i.e., right in the time window of 2D NMR, and simulate the spectra for different echo delays. The results are compiled in Fig. 8. Clearly, the lineshape of the spectra changes if t_p is extended although a $\tau \gg T_2^*$ is chosen. On the other hand, such changes do not appear, simulating an isotropic random jump with the same correlation time τ = 100 ms as a reference. This is evident inspecting the 1D spectrum found for that kind of motion and t_p = 200 μs displayed in Fig. 8, too. The differences between both models can be understood comparing the jump correlation times τ_j. Whereas τ_j equals τ for the isotropic random jump, a much smaller τ_j = 411 μs corresponds to the used correlation time for the isotropic 3° jump. Therefore, in contrast to the random jump, considering the latter model molecular dynamics takes place during the solid-echo pulse sequence which can lead to effects in the 1D spectra. We note that, applying large t_p and looking at an isotropic 15° jump characterized by τ = 1 ms and τ_j = 100 μs, changes in the lineshape are observed which are similar to those for the isotropic 3° jump displayed in Fig. 8.

If the 1D lineshape for large t_p is affected by molecular dynamics one will expect a dependence on the correlation time. This can be checked by calculating 1D spectra for various $\tau > T_2^*$ and a fixed echo delay t_p = 100 μs. The spectra obtained for the model of an isotropic 3° jump are shown in Fig. 9. Indeed, a distinct dependence of the lineshape on τ is obvious. Looking at a correlation time of 1 s a spectrum typical of rigid molecules is observed. Of course, this is reasonable since the corresponding τ_j amounts to about 4.1 ms and, thus, molecular dynamics during the pulse sequence is negligible. In other words, case 1 is valid for this correlation time. On the other hand, inspecting the spectra for correlation times in the millisecond regime changes in the lineshape are found which are the more pronounced the smaller τ. They are brought about by elementary jumps which occur during the pulse sequence when considering such τ for an isotropic 3° jump. For these pairs τ and τ_j, case 2 is met. These findings demonstrate that the 1D spectra shown are indeed influenced by molecular dynamics although $\tau > T_2^*$ is valid.

Summarizing, two prerequisites have to be fulfilled in order to obtain lineshape changes for $\tau > T_2^*$. First, the condition $\tau_j < T_2^*$ (case 2) must hold. Concerning the mechanism of reorientation, this means that the loss of correlation has to be achieved gradually by many elementary small angle jumps taking place one after another. Second, it is essential to apply large echo delays t_p. The long echo delays are necessary because considering $\tau > T_2^*$ at most a few elementary small angle jumps occur during the solid-echo sequence and, hence, the NMR frequency ω_Q is shifted just a little. The connection

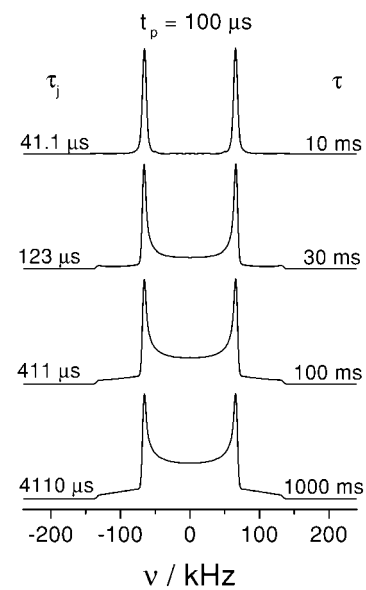

FIG. 9. RW simulations for the model of an isotropic 3° jump: 1D ^{2}H NMR spectra for various correlation times τ (solid-echo sequence: t_p = 100 μs).

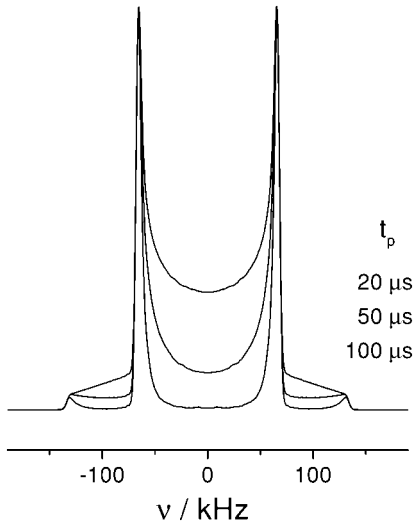

FIG. 10. RW simulations for the model of a random jump on a cone ($\chi = 6°$, $\tau = \tau_j = 30$ μs): 1D ^{2}H NMR spectra for the solid-echo sequence with various echo delays t_p.

between t_p and the amount of variation in ω_Q will be explained in detail below where the particular lineshape of the spectra will also be discussed. In conclusion we add that investigating the α process in supercooled liquids experimentally similar changes in the lineshape have been found for correlation times $\tau > T_2^*$ and large echo delays t_p (*16*, *43*). However, a systematic analysis of these 1D spectra comparing various types of isotropic dynamics is, to our knowledge, still missing.

3.2.2. Restricted dynamics: Exponential relaxation. As noted above, highly restricted dynamics can only be studied by applying 2D NMR in time domain if large evolution times t_p are chosen. Furthermore, it is well known that this kind of dynamics is difficult to observe in 2D NMR spectra because the ellipses resulting for such small angle fluctuations are hard to distinguish from diagonal intensity (*1*). Here, we want to investigate how highly restricted motions affect 1D ^{2}H NMR spectra. According to our goal we once again simulate reorientations on a cone with an opening angle $\chi = 6°$ as was done when considering 2D NMR in time domain.

First, we calculate 1D spectra assuming a random jump on this cone. Again, both τ and the echo delay t_p are varied in the simulations. We start keeping the jump correlation time fixed. The spectra for $\tau_j = \tau = 30$ μs and various t_p are shown in Fig. 10. If the echo delay is set to 20 μs a spectrum is found in which no effects of the considered motion can be recognized, although τ is chosen right in the time window of 1D NMR. This indicates that highly restricted dynamics cannot be observed in 1D spectra recorded in the ordinary way using small echo delays, as is well known from other investigations (*9*). However, applying larger echo delays, changes in the lineshape appear which are more pronounced the larger t_p as is clearly seen in Fig. 10. On the other hand, when fixing the echo delay at a large value a strong dependence of the spectra on the correlation time is found, too. For example, the changes in the lineshape for a $t_p = 100$ μs disappear using a $\tau_j = 1$ ms for the random jump on the cone, cf. Fig. 11b (RJ).

Analyzing the 1D spectra in Fig. 10 more precisely it becomes evident that mainly the intensity in the middle of the spectrum declines when extending t_p. In the following, we try to explain this finding on a qualitative level. Considering highly restricted motions the molecular orientation and, thus, the NMR frequency varies only a little. Obviously, these small changes in ω_Q are not sufficient to affect the 1D spectra for small t_p. This becomes clear when inspecting Eq. [2]. Provided that, at a time $t = t_p$, a small angle rotational jump causes a slight shift in frequency by $\Delta\omega_Q$, the phases $\phi(0, t_p)$ and $\phi(t_p, 2t_p)$ differ by $\Delta\omega_Q t_p$. Using a small t_p this phase shift is too little to affect the building of the echo significantly. However, increasing the echo delay leads to larger phase shifts $\Delta\omega_Q t_p$

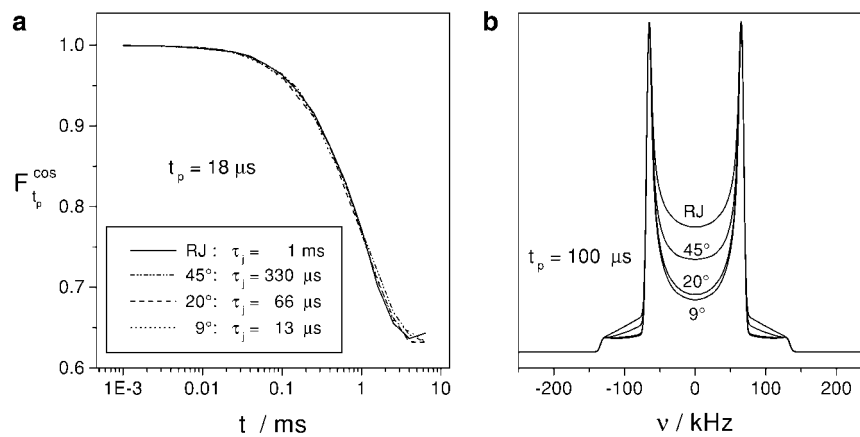

FIG. 11. RW simulations for the models of a random jump on a cone and of a rotational jump about various polar angles $\Delta\psi$ on a cone ($\chi = 6°$): (a) cos–cos correlation functions (four-pulse sequence: $t_p = 18$ μs, $\Delta = 15$ μs), inset: applied angles $\Delta\psi$ and jump correlation times τ_j; (b) 1D ^{2}H NMR spectra (solid-echo sequence: $t_p = 100$ μs) for the pairs ($\Delta\psi$, τ_j) indicated in (a).

and, consequently, to effects in the spectra. Therefore, it is plausible that, for highly restricted dynamics, changes in the lineshape can solely be observed by applying large t_p. Considering an isotropic 3° jump with a $\tau \gg T_2^*$, similar spectra were observed in Fig. 8. This is understood taking into account that, under these circumstances, a just as restricted area of the unit sphere is covered during the pulse sequence and, hence, our considerations hold for this kind of motion as well.

The particular lineshape of the 1D spectra for large t_p becomes clear taking into account the angular dependence of $\omega_Q(\theta)$, cf. Eq. [1]. Assuming for simplicity that the restricted motions change the molecular orientation during the solid-echo sequence by approximately the same small amount $\Delta\theta$, the resulting frequency shifts $\Delta\omega_Q$ depend only on the derivation of $\omega_Q(\theta)$. Comparatively large $\Delta\omega_Q$ and, hence, large phase shifts $\Delta\omega_Q t_p$ result for NMR frequencies where the curve $\omega_Q(\theta)$ is steep. As a consequence, molecules characterized by such initial ω_Q contribute less to the echo and the spectral intensity at these positions declines the most. Inspecting $\omega_Q(\theta)$ it is obvious that the curve is flat for $\theta \approx 0°$ and $\theta \approx 90°$ corresponding to the outer edges and the singularities, respectively, whereas it is steep for $\theta \approx 54°$ causing intensity in the middle of the spectrum. Therefore, the intensity in the latter part of 1D spectra is reduced in the presence of restricted motions.

Apart from the random jump, we now study reorientations on the cone which involve a constant polar angle $\Delta\psi$. Using this example, we want to demonstrate that restricted motions characterized by time constants $\tau > T_2^*$ and $\tau_j < T_2^*$ (case 2) cause changes in the 1D lineshape as well. Moreover, we want to investigate the dependence of the spectra on the jump angle $\Delta\psi$. However, when looking at this model one problem arises because the correlation time τ for a certain pair (τ_j, $\Delta\psi$) is not known a priori. This difficulty results from the fact that Eq. [8] is only valid for isotropic motions, but, of course, a dependence of τ on the jump angle $\Delta\psi$ is expected in our model, too. Nevertheless, τ can be roughly estimated considering in the RW simulations the correlation function for a evolution time t_p which, on the one hand, is large enough to lead to a distinct decay in the case of a restricted motion but, on the other, is as small as possible to still obtain a fair guess of τ. Here, we choose $t_p = 18$ μs.

According to our goal, we calculate 1D spectra resulting for motions on the cone which are characterized by different jump angles $\Delta\psi$ but a similar τ of about 1 ms. Here, we choose $\Delta\psi =$ 9, 20, and 45°. In order to obtain a comparable correlation time when using different $\Delta\psi$ we simulate the cos–cos correlation functions for $t_p = 18$ μs varying τ_j until a time constant $\tau_{t_p}^{app} =$ 1 ms is observed, respectively. The decays are displayed in Fig. 11a where the resulting τ_j are indicated as well. Using these pairs (τ_j, $\Delta\psi$) we calculate the 1D spectra corresponding to an echo delay $t_p = 100$ μs, cf. Fig. 11b. For comparison, the spectrum found assuming a random jump with $\tau = \tau_j = 1$ ms is included, too. Obviously, completely different lineshapes result for the considered models. Whereas in the case of a random jump a spectrum typical of rigid C–D bonds is observed, distinct changes in the lineshape are seen for rotational jumps about constant angles $\Delta\psi$. The observed changes are similar to those in Fig. 10. Further, they are more pronounced the smaller $\Delta\psi$. The latter finding becomes reasonable inspecting the jump correlation times τ_j corresponding to various angles $\Delta\psi$. Of course, considering smaller angles, shorter τ_j must be used to obtain a similar correlation function, cf. Fig. 11a. Therefore, the smaller $\Delta\psi$ the more molecular reorientations take place on the time scale of the solid-echo sequence and, consequently, the more strongly the lineshape is affected.

All together, it has turned out that highly restricted motions can be studied by recording 1D NMR spectra if large echo delays t_p are applied in the solid-echo sequence. Moreover, similar to the results for isotropic motions, we have found changes in the lineshape of these spectra even for $\tau > T_2^*$ provided that case 2 is valid, i.e., $\tau_j < T_2^*$. The latter result once again demonstrates that with measuring correlation functions and 1D spectra simultaneously further information about the mechanism of molecular reorientation is available, which will be particularly important when investigating the β process in supercooled liquids and glasses (*21, 42*).

4. CONCLUSION

By carrying out RW simulations we have calculated 1D ^{2}H NMR spectra and the results of 2D ^{2}H NMR experiments in time domain for various dynamical models. Until now, the latter experiment was mainly applied to measure the correlation function f_2 for ultraslow motions. Here, we have systematically studied whether this technique can also be used to determine the corresponding correlation time τ when considering faster dynamics. It has turned out that one has to distinguish between exponential relaxation and nonexponential relaxation caused by a distribution of correlation times $G(\lg\tau)$. Concerning exponential relaxation we have shown that also correlation times $\Delta \leq \tau < T_2^*$ can be measured by applying 2D ^{2}H NMR in time domain if an extended phase cycle (*28*) is used. Therefore, the time window of this experiment is enlarged by approximately 2 decades and a dynamical range becomes accessible for 2D NMR which was reserved for a lineshape analysis of 1D NMR spectra in the past. However, the situation changes if there is a distribution of correlation times $G(\lg\tau)$. Then, the resulting nonexponential correlation function f_2 is not properly measured by 2D NMR as soon as the distribution contains correlation times $\tau < T_2^*$. This finding is understood taking into account that magnetization of molecules with $\tau < T_2^*$ is not completely refocused in the applied four-pulse sequence and that, hence, various parts of $G(\lg\tau)$ do not uniformly contribute to the measured signal. However, knowing the mechanism of molecular reorientation these effects can be calculated. Consequently, it is, despite the described problems, useful to apply mixing times which are as short as possible.

Strictly speaking, in the presence of a distribution $G(\lg\tau)$, deviations between real and measured correlation function will appear if some of the jump correlation times τ_j out of the corresponding distribution $G(\lg\tau_j)$ are on the order of the delays t_p and Δ, respectively. Thus, one has to be particularly careful when investigating motions like the α process in supercooled liquids which are characterized by a distribution of correlation times and for which the loss of correlation is achieved by rotational jumps about small angles since τ_j is much shorter than τ in this case. This caution is even more important if large evolution times $t_p \gg \Delta$ are used to determine the value of the elementary jump angle by carrying out 2D NMR experiments in time domain. For this kind of measurement one has to ensure that all appearing τ_j are long with respect to the applied evolution times t_p in order to obtain correct results.

Furthermore, we have investigated the effects of highly restricted dynamics on 2D NMR experiments in time domain. Such small amplitude reorientations can clearly be observed if large evolution times t_p are applied. For short t_p and, thus, in f_2, of course only a very small amount of correlation is lost. Therefore, it is generally, independent of its actual value, very difficult to determine the correlation time τ of highly restricted motions. A puzzling situation appears if a distribution $G(\lg\tau)$ broader than the experimental time window is taken into account. In this case, the time constant of the correlation function for a sufficiently large t_p is only slightly affected by a strong shift of $G(\lg\tau)$ but it is to a high extent given by the time window of the 2D experiment itself. Nevertheless, a rough estimate of the position of $G(\lg\tau)$ is available by analyzing the amount of loss which is achieved in the measured correlation function. Although these results have explicitly been obtained for restricted dynamics, we expect similar observations for other motions and short t_p.

Using RW simulations we have moreover demonstrated that molecular dynamics with correlation times $\tau > T_2^*$, in NMR usually studied by applying multidimensional techniques, can simultaneously be investigated by recording 1D NMR spectra provided that the condition $\tau_j < T_2^*$ is fulfilled for the jump correlation time. In other words, case 2 has to be valid. Concerning the mechanism of the considered motion the latter requirement means that the loss of correlation must be achieved gradually because only then a distinct separation of the time scales of τ and τ_j is obtained. Furthermore, one has to apply sufficiently large echo delays t_p in order to make the effects of the elementary rotational jumps visible in the spectrum. These remarks hold, similarly, for isotropic and for highly restricted motions. However, shifting the time constant into the regime $\tau < T_2^*$, i.e., considering case 3, both kinds of dynamics manifest themselves differently. Of course, looking at isotropic and anisotropic large angle reorientations on this time scale, changes in the spectral lineshape can be observed for short t_p as well [3]. On the other hand, highly restricted motions even then do not affect 1D NMR spectra measured with short echo delays. Instead, large t_p must be used to detect this dynamics anyway.

All together, we have shown that the time windows of different NMR techniques which were assumed to be fixed in most prior work become indistinct when studying complex molecular dynamics. In this case, they depend not only on the correlation time τ but also on the mechanism of the considered molecular dynamics. In particular, when investigating motions where the loss of correlation is achieved step by step, the jump correlation time τ_j must be taken into account as well. For example, if τ and τ_j differ by many orders of magnitude it is possible that the same small step motion simultaneously manifests itself in T_1, 1D, and 2D NMR experiments. Therefore, carrying out all these measurements at the same time yields additional information about molecular dynamics since one dynamical model must describe all resulting NMR observables. Such a simultaneous description is, on the one hand, a very challenging task and, on the other, it demonstrates that NMR is a powerful tool when revealing the mechanism of complex molecular dynamics.

We close with the remark that RW simulations have proven to be well suited to calculating the results of 1D and 2D ^{2}H NMR experiments in the presence of complex molecular dynamics. In particular, simulating 1D ^{2}H NMR spectra for such motions is a straightforward task. Although all RW simulations have been carried out for the special case of ^{2}H NMR, it is expected that similar results will be observed considering other nuclei with a dominating single particle interaction like ^{13}C or ^{31}P.

REFERENCES

1. K. Schmidt-Rohr and H. W. Spiess, "Multidimensional Solid-State NMR and Polymers," Academic Press, London, 1994.
2. H. W. Spiess, *J. Chem. Phys.* **72,** 6755 (1980).
3. H. W. Spiess and H. Sillescu, *J. Magn. Reson.* **42,** 381 (1981).
4. D. Hentschel, H. Sillescu, and H. W. Spiess, *Polymer* **25,** 1078 (1984).
5. C. Schmidt, K. J. Kuhn and H. W. Spiess, *Progr. Colloid Polymer Sci.* **71,** 71 (1985).
6. D. E. Wemmer, D. J. Ruben, and A. Pines, *J. Am. Chem. Soc.* **103,** 28 (1981).
7. H. W. Spiess, *Colloid Polymer Sci.* **261,** 193 (1983).
8. A. K. Roy, A. A. Jones, and P. T. Inglefield, *J. Magn. Reson.* **64,** 441 (1985).
9. M. Wehrle, G. P. Hellmann, and H. W. Spiess, *Colloid Polymer Sci.* **265,** 815 (1987).
10. M. S. Greenfield, A. D. Ronemus, R. L. Vold, R. R. Vold, P. D. Ellis, and T. E. Raidy, *J. Magn. Reson.* **72,** 89 (1987).
11. F. Fujara, S. Wefing, and H. W. Spiess, *J. Chem. Phys.* **84,** 4579 (1986).
12. E. Rössler, *Chem. Phys. Lett.* **128,** 330 (1986).
13. F. Fujara, S. Wefing, and W. F. Kuhs, *J. Chem. Phys.* **88,** 6801 (1988).
14. C. Schmidt, S. Wefing, B. Blümich, and H. W. Spiess, *Chem. Phys. Lett.* **130,** 84 (1986).

15. C. Schmidt, B. Blümich, and H. W. Spiess, *J. Magn. Reson.* **79,** 269 (1988).
16. U. Pschorn, E. Rössler, H. Sillescu, S. Kaufmann, D. Schaefer, and H. W. Spiess, *Macromolecules* **24,** 398 (1991).
17. B. Geil, F. Fujara, and H. Sillescu, *J. Magn. Reson.* **130,** 18 (1998).
18. G. Hinze, *Phys. Rev. E* **57,** 2010 (1998).
19. R. Böhmer and G. Hinze, *J. Chem. Phys.* **109,** 241 (1998).
20. U. Tracht, A. Heuer, and H. W. Spiess, *J. Chem. Phys.* **111,** 3720 (1999).
21. M. Vogel and E. Rössler, in preparation.
22. G. Diezemann and H. Sillescu, *J. Chem. Phys.* **111,** 1126 (1999).
23. Proceedings of the International Discussion Meeting on Relaxation in Complex Systems II, *J. Non-Cryst. Solids* **172–174** (1994).
24. R. Böhmer, R. V. Chamberlin, G. Diezemann, B. Geil, A. Heuer, G. Hinze, S. C. Kuebler, R. Richert, B. Schiener, H. Sillescu, H. W. Spiess, U. Tracht, and M. Wilhelm, *J. Non-Cryst. Solids* **235–237,** 1 (1998).
25. A. Heuer, J. Leisen, S. C. Kuebler, and H. W. Spiess, *J. Chem. Phys.* **105,** 7088 (1996).
26. G. P. Johari and M. Goldstein, *J. Chem. Phys.* **55,** 4245 (1971).
27. A. Kudlik, C. Tschirwitz, S. Benkhof, T. Blochowicz, and E. Rössler, *Europhys. Lett.* **40,** 649 (1997).
28. D. Schaefer, J. Leisen, and H. W. Spiess, *J. Magn. Reson.* **115,** 60 (1995).
29. S. Kaufmann, S. Wefing, D. Schaefer, and H. W. Spiess, *J. Chem. Phys.* **93,** 197 (1990).
30. D. Schaefer and H. W. Spiess, *J. Chem. Phys.* **97,** 7944 (1992).
31. J. Jeener and P. Broekaert, *Phys. Rev.* **157,** 232 (1967).
32. E. N. Ivanov, *Soviet Physics JETP* **18,** 1041 (1964).
33. A. Abragam, "The Principles of Nuclear Magnetism," Oxford Univ. Press, London, 1961.
34. N. G. van Kampen, "Stochastic Processes in Physics and Chemistry," North-Holland, Amsterdam, 1981.
35. M. Vogel and E. Rössler, *J. Phys. Chem.* **102,** 2102 (1998).
36. Th. Blochowicz, C. Karle, A. Kudlik, P. Medick, I. Roggatz, M. Vogel, Ch. Tschirwitz, J. Wolber, J. Senker, and E. Rössler, *J. Phys. Chem.* **103,** 4032 (1999).
37. J. E. Anderson, *Faraday Symp. Chem. Soc.* **6,** 82 (1972).
38. M. Bloom, J. H. Davis, and M. I. Valic, *Can. J. Phys.* **58** (1980).
39. R. Kohlrausch, *Pogg. Ann. Phys.* **4,** 56 (1854).
40. G. Williams and D. C. Watts, *Trans. Faraday Soc.* **66,** 80 (1970).
41. P. Medick, Diploma thesis, Universität Bayreuth, Germany, 1998.
42. M. Vogel and E. Rössler, *J. Phys. Chem. B* **104,** 4285 (2000).
43. E. Rössler, Ph.D. thesis, Universität Mainz, Germany, 1984.